Letter

Disentangling the electronic and lattice contributions to the dielectric response of photoexcited bismuth

F. Thiemann [1,*] G. Sciaini [2] A. Kassen,[1] T. S. Lott [2] and M. Horn-von Hoegen [1,3]

[1]*Department of Physics, University of Duisburg-Essen, Lotharstrasse 1, 47057 Duisburg, Germany*

[2]*Department of Chemistry, The Ultrafast Electron Imaging Lab, and Waterloo Institute for Nanotechnology, University of Waterloo, Waterloo, Ontario, Canada N2L 3G1*

[3]*Center for Nanointegration (CENIDE), University of Duisburg-Essen, Carl-Benz-Strasse 199, 47057 Duisburg, Germany*

(Received 21 June 2023; revised 10 October 2023; accepted 18 December 2023; published 16 January 2024)

Elucidating the interplay between nuclear and electronic degrees of freedom that govern the complex dielectric behavior of materials under intense photoexcitation is essential for tailoring optical properties on demand. However, conventional transient reflectivity experiments have been unable to differentiate between real and imaginary components of the dielectric response, omitting crucial electron-lattice interactions. Utilizing thin film interference we unambiguously determine the photoinduced change in the complex dielectric function in the Peierls semimetal bismuth and examine its dependence on the excitation density and nuclear motion of the A_{1g} phonon. Our modeled transient reflectivity data reveal a progressive broadening and redshift of Lorentz oscillators with increasing excitation density and underscores the importance of both electronic and nuclear coordinates in the renormalization of interband transitions.

DOI: 10.1103/PhysRevB.109.L041105

Currently, ultrashort light pulses remain as powerful probes for monitoring a variety of out-of-equilibrium dynamics through sudden changes of the optical dielectric properties within the photoexcited material [1,2]. In particular, a detailed examination of the dielectric function provides further insights, such as the electron-phonon coupling strength in metals [3] and the identification of exciton properties in transition metal dichalcogenides [4]. Although these effects are also accessible through other experimental techniques, the main advantage of qualitatively understanding how these affect the optical response is the ability to manipulate the latter by changing electron or lattice degrees of freedom. However, the complexity of the dielectric response escalates as the number of degrees of freedom participating increases. Disentangling these intertwined contributions presents one of the current challenges in ultrafast science [5,6]. In particular, the various degrees of freedom in correlated materials like VO_2, TiS_2, especially layered ones like TaS_2 [7] and other charge density wave (CDW) compounds [8,9] or group V semimetals [10] are of broader interest. To target this topic a wealth of transient reflectivity studies were conducted in the semimetal bismuth (Bi) [2,11–15], known for its intrinsic Peierls distortion [16], low carrier density [17], and small effective mass [18]. When photoexcited, Bi undergoes a significant increase in carrier density, resulting in a transient modification of the atoms' potential energy surface, which, in turn, launches coherent A_{1g} phonons [19–21]. Despite this body of work, the interconnection between carrier and nuclear dynamics and the dielectric response remains unclear [22].

Here, we study the change of the complex dielectric function $\Delta\varepsilon(\hbar\omega)$ upon impulsive photoexcitation through broadband femtosecond (fs) transient reflectivity. Measurements were carried out on a series of (111)-oriented Bi films [23,24] epitaxially grown on Si(111). Film thicknesses d of 17, 28, 39, 42, and 197 nm allow us to exploit interference effects and obtain an unambiguous solution for the lattice and electronic contributions to the transient dielectric function. Based on the geometry and crystal orientation used in our experiment we only study the ordinary dielectric function [25].

The films were excited by 160-fs optical pulses with a central wavelength of $\lambda = 800$ nm (1.55 eV) in normal incidence, providing a maximum absorbed fluence of 0.23 mJ/cm^2. The optical response of Bi was probed by time delayed, Δt, white light pulses (p-polarized, 32° incidence). Transient reflectivity changes $\Delta R/R_0(\hbar\omega, \Delta t)$ in the range of $\lambda = 580$ nm to 700 nm (2.1 eV to 1.8 eV) were recorded using a dispersive spectrometer. *Ex situ* ellipsometry (see Supplemental Material [26]) was used to verify the thickness of the Bi films on silicon and the consistency of the optical properties in comparison with existing studies [25,27].

Figure 1(a) shows a typical time-resolved broadband transient reflectivity spectrum $\Delta R/R_0(\hbar\omega, \Delta t)$ obtained from the 17-nm-thick Bi film with characteristics such as the initial sharp jump of reflectivity, the oscillations at ≈ 3 THz, and the decaying background. The spectral dependence exhibits a minimum around 2 eV. For further analysis, we applied a moving average window with a width of 0.015 eV (teal line). Temporal traces within Δt (−0.5 ps to 1.0 ps) are shown in Fig. 1(b) for five different Bi film thicknesses at a photon energy of $\hbar\omega = 1.9$ eV and an incidence fluence of 0.9 mJ/cm^2. It is noteworthy that the transients exhibit a flip of sign in their oscillation amplitude between 28 nm $< d <$ 39 nm.

*fabian.thiemann@uni-due.de

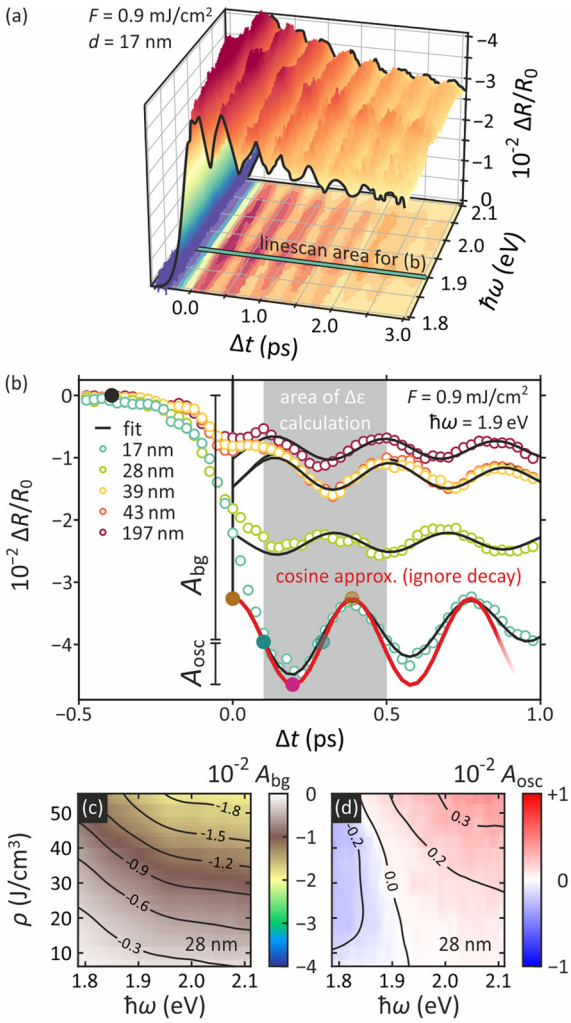

FIG. 1. (a) $\Delta R/R_0(\Delta t, \hbar\omega)$ for a 17-nm-thick Bi film. (b) Temporal traces, averaged across the teal line in (a), obtained at a photon energy of 1.9 eV for films of different thickness. The grey area marks where the calculation of $\Delta\varepsilon$ was conducted. The black lines mark the fits obtained with the model described in Eq. (1). The large colored dots refer to distinct points in the potential energy surface of the distorted lattice [see Fig. 2(a)]. (c), (d) show the amplitudes A_{bg} and A_{osc}, as indicated by the solid black bars in panel (b), for the 28-nm-thick film.

Since the reflectivity change $\Delta R/R_0(\Delta t, d)$ is the essential input for the calculation of the dielectric function change $\Delta\varepsilon$, we systematically describe it by fitting a phenomenological model [28] for all thicknesses d, photon energies $\hbar\omega$, and pump fluences F as follows:

$$\frac{\Delta R}{R_0}(t) = A_{\mathrm{bg}}\, e^{-\frac{t}{\tau_{\mathrm{bg}}}} + A_{\mathrm{osc}}\, e^{-\frac{t}{\tau_{\mathrm{osc}}}} \cos(\Omega t). \qquad (1)$$

The model consists of two terms, the first one describing the decaying background with initial amplitude A_{bg} and time constant τ_{bg}. The second one representing the oscillations arising from A_{1g} phonons, with initial amplitude A_{osc}, dephasing time constant τ_{osc}, and angular frequency Ω. The last of these was obtained independently by Fourier analysis and found to change linearly with fluence. The terms are usually referred to as "electronic" and "phononic" [29–31]. Such references are not used in this work because, in general, both parts include carrier and lattice contributions.

The incident fluence F is an inappropriate parameter to compare the excitation in layers of different thicknesses d. In a previous work [32] we demonstrated that ultrafast transport of nonthermalized carriers redistributed the excitation throughout thin films ($d < 60$ nm) within 150 fs after excitation. Afterwards the film is homogeneously excited, quantified by the absorbed energy density $\rho = F_{\mathrm{abs}}/d$, where d is either the film thickness or the effective carrier skin depth d_{eff} as introduced in Ref. [33] and F_{abs} the absorbed fraction of incident fluence. Within the time window of 150 fs to 500 fs [grey area in Fig. 1(b)] and for the sake of a simple analysis we approximate the transients of $\Delta R/R_0(\Delta t, \rho)$ by a cosine with the amplitude A_{osc} and offset A_{bg}, excluding the decays described by τ_{bg} and τ_{osc}. They can be ignored in our analysis because the cooling [34] and dephasing behavior [14,35] depends on d and the thermalized excited carriers remain at the valence band maximum (T-point) and the conduction band minimum (L-point) for a few ps prior to recombination [22], respectively. The amplitudes $A_{\mathrm{osc}}(\rho, \hbar\omega)$ and $A_{\mathrm{bg}}(\rho, \hbar\omega)$, interpolated to the same ρ, are shown in Figs. 1(c) and 1(d). The most characteristic pattern of $A_{\mathrm{osc}}(\rho, \hbar\omega)$, observed for the 28-nm film, features the flip of sign in the ρ-$\hbar\omega$-plane, similar to the one in Fig. 1(b) for different film thicknesses.

Owing to the cosine approximation for $\Delta R/R_0(\Delta t)$, it is sufficient to recover the change of dielectric function $\Delta\varepsilon$ at the two extrema and the node of the oscillations. Thus $A_{\mathrm{bg}} + A_{\mathrm{osc}}$, A_{bg}, and $A_{\mathrm{bg}} - A_{\mathrm{osc}}$ refer to the dielectric function changes $\Delta\varepsilon_0$, $\Delta\varepsilon_{\mathrm{q-eq}}$, and $\Delta\varepsilon_\pi$ at the three indicated positions. q-eq denotes the new quasi-equilibrium position and the phases $\varphi = 0$ and $\varphi = \pi$ describe the maxima and minima of the oscillation. The three distinct points are marked in the potential energy surface (described in Ref. [36]) by colored dots (see Fig. 2).

The dielectric function change $\Delta\varepsilon$ is obtained by fitting $\Delta R/R_0(\Delta\varepsilon, d, \hbar\omega)$ at the three distinct points in the potential energy surface. Because $\Delta R/R_0$ is connected to $\Delta\varepsilon$ by the absolute square and all complex information is lost, an unambiguous solution for $\Delta\varepsilon$ is only obtained by providing additional information. This can be transmission [3], polarization [37–39], incident angle [39–41], or in this case the film thickness d. The use of d is only reasonable when thin film interference causes significant changes of $\Delta R/R_0$ within a regime of d where the films are homogeneously excited. We can exclude any optical property changes of the Si substrate as a Schottky barrier at the Bi/Si interface [42] prevents its excitation. The formation of the Bi surface state is prevented by the formation of a 3 -nm-thick oxide layer [24]. Quantum confinement effects are negligible for the film thicknesses studied herein [43]. Therefore, $\Delta R/R_0(\Delta\varepsilon, d, \hbar\omega)$ is computed solely with the Fresnel coefficient at the air/Bi and Bi/Si interfaces, d, and the dielectric function change in the bismuth film $\Delta\varepsilon$ by using the transfer matrix method [44].

The individual panels in Fig. 2(e) exemplarily show the solutions, indicated by the fits' residuals $|A_{\mathrm{bg}}(d) - \Delta R/R_0(d, \Delta\varepsilon)|$ for the change in the real and imaginary parts of the dielectric function for five different film thicknesses at the same $\hbar\omega = 2.1$ eV. No unambiguous

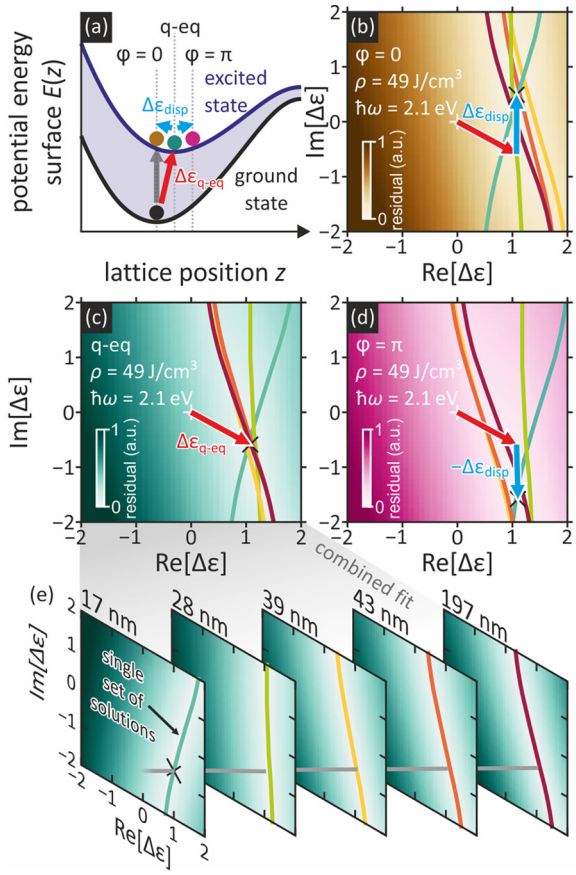

FIG. 2. (a) Bismuth's potential energy surface according to [36]. The colored dots refer to the positions of the oscillation shown in Fig. 1(b). The grey arrow marks the pathway of excitation. The red and blue arrows indicate the changes to the quasi-equilibrium position (q-eq) and the displacive component (disp) respectively. [(b)–(d)] Combined residual for all films at the positions marked in (a). (e) Residuals of the fits for $\Delta\varepsilon(d)$ at the q-eq position.

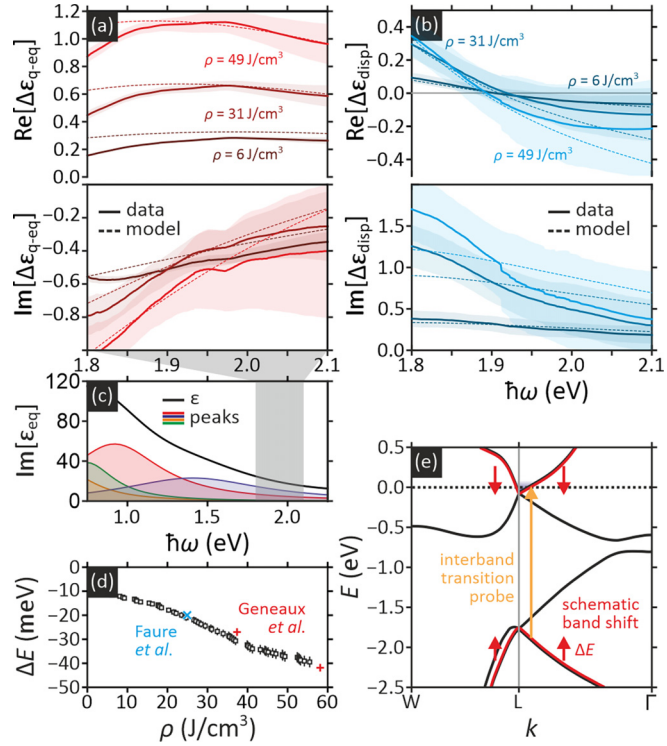

FIG. 3. (a) Change of real and imaginary part of $\Delta\varepsilon_{\mathrm{q-eq}}$ for selected absorbed energy densities ρ. Solid lines mark $\Delta\varepsilon$, the light-colored area the uncertainty, and the dashed lines the fitted model. (b) $\Delta\varepsilon_{\mathrm{disp}}$ for selected ρ. (c) Imaginary part of bismuth's dielectric function $\varepsilon_{\mathrm{eq}}$ (black), based on the model from Ref. [25]. The colored peaks are the single Lorentz peaks. (d) Peak shift fit parameter ΔE compared to expected estimated shifts from literature [58,59]. (e) Sketch of bismuth's band structure based on Ref. [45]. The orange arrow marks a possible probe interband transition. The blue area indicates population changes affecting the probe intensity. The shift observed in ΔE is caused by arbitrary band shifts, indicated in red.

solution for $\Delta\varepsilon = \mathrm{Re}[\Delta\varepsilon] + i\,\mathrm{Im}[\Delta\varepsilon]$ is obtained for each of the film thicknesses d, but a set of solutions in the Re[$\Delta\varepsilon$]-Im[$\Delta\varepsilon$]-plane [indicated by a solid line in Fig. 2(e)] that changes due to thin film interference. Based on the safe assumption that, at the same absorbed energy density, $\Delta\varepsilon$ is independent on film thickness d, the intersection of these individual solutions (grey line) yields the unambiguous solution for $\Delta\varepsilon$.

Figures 2(b)–2(d) summarize this procedure for $\Delta\varepsilon_0$, $\Delta\varepsilon_{\mathrm{q-eq}}$, and $\Delta\varepsilon_\pi$. Correspondingly to Fig. 2(e), the colored lines mark the individual solutions for each film thickness d while the cross identifies the overall minimum of the combined residuals $\sum_d |A(d) - \Delta R/R_0(d, \Delta\varepsilon)|$. Across Fig. 2, $\Delta\varepsilon_{\mathrm{q-eq}}$ is emphasized by red arrows. It is useful to define a displacive component $\Delta\varepsilon_{\mathrm{disp}}$ (blue arrows in Fig. 2), including only the changes from q-eq towards the maximum ($\varphi = 0$) and minimum ($\varphi = \pi$) displacement within the potential energy surface. $\Delta\varepsilon_{\mathrm{disp}}$ is modulated solely by the nuclear motion in an excited state. Because of the cosine approximation $\Delta\varepsilon_{\mathrm{disp}}$ is symmetric:

$$\Delta\varepsilon_{\mathrm{disp}} = \Delta\varepsilon_0 - \Delta\varepsilon_{\mathrm{q-eq}} = -\Delta\varepsilon_\pi + \Delta\varepsilon_{\mathrm{q-eq}}. \qquad (2)$$

This procedure to obtain $\Delta\varepsilon$ was performed for all film thicknesses d, photon energies $\hbar\omega$, and absorbed energy densities ρ at the positions q-eq and disp, yielding an indigestible multi dimensional parameter space. Displaying only selected energy densities ρ provides more insight. Figure 3(a) shows $\Delta\varepsilon_{\mathrm{q-eq}}(\hbar\omega)$ for selected ρ and Fig. 3(b) $\Delta\varepsilon_{\mathrm{disp}}(\hbar\omega)$, respectively. The solid lines in Figs. 3(a) and 3(b) depict the real and imaginary parts of $\Delta\varepsilon(\hbar\omega)$. The light-colored areas mark the regime of uncertainty obtained from the fits. Figure 3(c) shows the imaginary part of the equilibrium dielectric function $\varepsilon_{\mathrm{eq}}$ obtained over a broader spectral range by ellipsometry measurements based on a model taken from the literature [25].

The next step is to provide a model for the observed changes in the dielectric function $\Delta\varepsilon_{\mathrm{q-eq}}$ and $\Delta\varepsilon_{\mathrm{disp}}$ that gives insight into the transient electronic dynamics in the material. Since the overall excitation densities ρ are weak and hence the deviations from equilibrium are small, we construct a simple model by changing the dielectric function under equilibrium conditions

$$\varepsilon(\rho) = \varepsilon_{\mathrm{eq}} + \Delta\varepsilon_{\mathrm{q-eq}}(\rho) + \Delta\varepsilon_{\mathrm{disp}}(\rho). \qquad (3)$$

Drude or intraband contributions (dominant in metals) are negligible for Bi in the range of visible light [22] and thus $\varepsilon_{\mathrm{eq}}$

is mainly defined by interband transitions [25,46,47] In such cases the Lorentz oscillator model [48–51] is often used and defined as the sum of single complex Lorentz peaks that obey the Kramers-Kronig relation

$$\varepsilon_{\mathrm{eq}}(\hbar\omega) = \sum_j \frac{A_j \Gamma_j, E_j}{E_j^2 - \hbar\omega^2 - i\Gamma_j \hbar\omega}, \tag{4}$$

with the parameters amplitude A_j, width Γ_j, and central energy E_j. The numerical values were taken from the literature [25] and agree with our ellipsometry data (see Supplemental Material [26]). Comparing the Lorentz peaks with the spectral window studied [see Fig. 3(c)], we notice that only the tails of two oscillators are important. In a simple picture the oscillators refer to interband transitions with large spectral weight in the band structure.

First, we consider only the influence of the excited charge carriers under a slightly weakened Peierls distortion of the lattice at the new quasi-equilibrium position (q-eq), treating the system as if there were no coherent phonons. The modification of Lorentz oscillators has proven to describe the impact of population changes and band shifts in the optical properties, as recently demonstrated in transition metal dichalcogenides [4,52,53]. In most materials the parameters of the Lorentz oscillators do not vary much throughout a broad spectral range [54–57] and since our spectral range is comparatively small, we have to approximate the change of all Lorentz peaks with three parameters only: $A_j \to f_A A_j$, $\Gamma_j \to f_\Gamma \Gamma_j$, and $E_j \to E_j + \Delta E$. They are determined by fitting the modified Lorentz oscillators (dashed lines) to the data shown in Fig. 3(a) for each corresponding ρ. The change in ΔE as a function of energy density is shown in Fig. 3(d) and compared to the extracted estimated relative shift between valence and conduction bands in recent studies perfomed with time-resolved angle-resolved photoemission spectroscopy (tr-ARPES) [58] and time-resolved extreme ultraviolet (tr-XUV) spectroscopy [59]. We find that the Lorentz peaks decrease in amplitude, broaden, and redshift in energy. This result is very close to the general behavior of the parameters A_j, Γ_j, and E_j, describing the change in dielectric function in semiconductors upon changes in temperature as observed for Si, Ge, and GaAs [54–57].

In these references, however, the carriers are thermally and not optically excited and band structure changes arise from thermal lattice expansion instead of a modified Peierls-like distortion. This is still comparable to our situation because in Bi optically excited electrons are quasithermalized 150 fs after excitation [58], matching the time window studied [see Fig. 1(b)]. Also, the lattice changes induced by thermal heating are related to a reduction of the Peierls distortion and softening of the energy surface, respectively [60]. Furthermore, we can compare our results to energy shifts ΔE observed in tr-ARPES [58] and UV-absorption spectroscopy studies [59]. Both, compared to the fitted ΔE, exhibit the same trend and the same order of magnitude, while absolute values are hard to compare due to the ambiguity of excited carrier density [32,33].

The relation between the behavior of excited carriers ΔE and the modification of peak amplitudes and widths can be explained in the band structure picture as sketched around the L-point in Fig. 3(e). This allows for the extraction of transient band shifts for, e.g., the semiconductor Te, which also exhibits a Peierls distortion, by Kudryashov *et al.* [48,49] or in later studies by Shih *et al.* [61] and Richter *et al.* [38] for ZnO. Population dynamics upon photoexcitation lead to bleaching and thus to changes of the maximum in $\mathrm{Re}[\Delta\varepsilon_{\mathrm{q-eq}}]$ around 2 eV. During thermalization the carriers relax to the band edge and accumulate at the L-point (electrons) and T-point (holes) after 150 fs, respectively [58]. This region is exactly covered by our spectral range. The $L_a(2) \to L_s(3)$ transition [orange arrow in Fig. 3(e)] connects an occupied valence band to this partially occupied conduction band minimum, $\Delta E \approx 2$ eV apart [17,45,47,62]. With this transition bleached by excited carriers, thus reducing the availability of final states, the absorption decreases the strongest at $\approx$2 eV. Furthermore, the increased peak width can be understood in a two-temperature model through the smeared-out Fermi-distribution of the thermalized but still hot carriers [63].

Moving on to the displacive component $\Delta\varepsilon_{\mathrm{disp}}$. In general, the phonon influence on the electronic properties is often modeled with a deformation potential approach [64] and was successfully applied to the correlated material Te [48,49]. Based on previous studies in semimetals, namely, Sb by Stevens *et al.* [65], which treated the coherent phonon excitations without excitation of the electron system, we would expect a Raman correction term that results from adding the electron-phonon interaction to the Hamiltonian like in the general approach. This term, $\Delta\varepsilon_{\mathrm{disp}} = \chi_R Q(t = 2\pi/\Omega)$, is described by the Raman susceptibility χ_R and the phonon coordinate $Q(t)$. The Raman susceptibility χ_R can be described in terms of a second-order nonlinear interaction between the probe light and a "phonon field," which is coupled to the electron system via the electron-phonon coupling Ξ. Using the simplifications $\Omega \ll \omega$ and $\Xi = \mathrm{const.}$ [65,66], we obtain

$$\Delta\varepsilon_{\mathrm{disp}} = \chi_R Q \approx \frac{\Xi Q}{4\pi\hbar} \frac{\mathrm{d}}{\mathrm{d}\omega} \varepsilon_{\mathrm{eq}}. \tag{5}$$

In contrast, we find the nonempirical relation

$$\Delta\varepsilon_{\mathrm{disp}} \propto \frac{\mathrm{d}}{\mathrm{d}\omega} \Delta\varepsilon_{\mathrm{q-eq}}, \tag{6}$$

which seems to depend on the quasi-equilibrium component or the change of $\varepsilon_{\mathrm{eq}}$ in general. An explanation might be that population changes at the L-point in Sb do not strongly affect interband transitions around 2 eV, as in bismuth. Additionally, the assumption $\Xi = \mathrm{const.}$ may not necessarily hold, and the previous simplification does not account for population changes. Therefore, we hypothesize that the population of excited carriers plays a significant role in the description of optical properties changes by coherent phonons in Bi. Proposing a first-principle's solution to this open question based on the available data set would be highly speculative, but a possible starting point would be a modeling of the dielectric function with the Lorentz model at each given time delay like in the works by Kudryashov *et al.* [48,49].

In summary, we tracked the changes in the complex dielectric function $\Delta\varepsilon$ of photoexcited Bi and separated it into a quasi-equilibrium and a displacive structural component, incorporating the carrier and lattice dynamics. These contributions were analyzed using a phenomenological

approach. A modified Lorentz oscillator model revealed a substantial impact of the interband transition to the conduction band minimum at the *L*-point, and the effects of the electron gas temperature and Pauli blocking on the optical properties of this strongly correlated system.

We gratefully acknowledge fruitful discussions with R. Géneaux, R. Merlin, M. Henstridge, and A. von Hoegen. This work was funded by the Deutsche Forschungsgemeinschaft (DFG, German Research Foundation) Project No. 278162697–SFB 1242. G.S. acknowledges the support of the National Science and Engineering Research Council of Canada (Project No. RGPIN-2020-06474), the Canada Foundation for Innovation and Ontario Research Fund (Project No. 33333).

The authors declare no competing financial interest.

[1] R. W. Schoenlein, W. Z. Lin, J. G. Fujimoto, and G. L. Eesley, Femtosecond studies of nonequilibrium electronic processes in metals, Phys. Rev. Lett. **58**, 1680 (1987).

[2] T. K. Cheng, S. D. Brorson, A. S. Kazeroonian, J. S. Moodera, G. Dresselhaus, M. S. Dresselhaus, and E. P. Ippen, Impulsive excitation of coherent phonons observed in reflection in bismuth and antimony, Appl. Phys. Lett. **57**, 1004 (1990).

[3] M. Obergfell and J. Demsar, Tracking the time evolution of the electron distribution function in copper by femtosecond broadband optical spectroscopy, Phys. Rev. Lett. **124**, 037401 (2020).

[4] S. Calati, Q. Li, X. Zhu, and J. Stähler, Ultrafast evolution of the complex dielectric function of monolayer WS_2 after photoexcitation, Phys. Chem. Chem. Phys. **23**, 22640 (2021).

[5] S. Gerber, S.-L. Yang, D. Zhu, H. Soifer, J. A. Sobota, S. Rebec, J. J. Lee, T. Jia, B. Moritz, C. Jia, A. Gauthier, Y. Li, D. Leuenberger, Y. Zhang, L. Chaix, W. Li, H. Jang, J.-S. Lee, M. Yi, G. L. Dakovski *et al.*, Femtosecond electron-phonon lock-in by photoemission and x-ray free-electron laser, Science **357**, 71 (2017).

[6] M. R. Otto, L. P. R. de Cotret, D. A. Valverde-Chavez, K. L. Tiwari, N. Émond, M. Chaker, D. G. Cooke, and B. J. Siwick, How optical excitation controls the structure and properties of vanadium dioxide, Proc. Natl. Acad. Sci. USA **116**, 450 (2018).

[7] A. Mann, E. Baldini, A. Odeh, A. Magrez, H. Berger, and F. Carbone, Probing the coupling between a doublon excitation and the charge-density wave in TaS_2 by ultrafast optical spectroscopy, Phys. Rev. B **94**, 115122 (2016).

[8] J. Demsar, L. Forró, H. Berger, and D. Mihailovic, Femtosecond snapshots of gap-forming charge-density-wave correlations in quasi-two-dimensional dichalcogenides 1*T* - TaS_2 and 2*H* - $TaSe_2$, Phys. Rev. B **66**, 041101(R) (2002).

[9] S. Wall, D. Wegkamp, L. Foglia, K. Appavoo, J. Nag, R. Haglund, Jr., J. Stähler, and M. Wolf, Ultrafast changes in lattice symmetry probed by coherent phonons, Nat. Commun. **3**, 721 (2012).

[10] T. K. Cheng, J. Vidal, H. J. Zeiger, G. Dresselhaus, M. S. Dresselhaus, and E. P. Ippen, Mechanism for displacive excitation of coherent phonons in Sb, Bi, Te, and Ti_2O_3, Appl. Phys. Lett. **59**, 1923 (1991).

[11] M. Hase, K. Mizoguchi, H. Harima, S. Nakashima, M. Tani, K. Sakai, and M. Hangyo, Optical control of coherent optical phonons in bismuth films, Appl. Phys. Lett. **69**, 2474 (1996).

[12] M. F. DeCamp, D. A. Reis, P. H. Bucksbaum, and R. Merlin, Dynamics and coherent control of high-amplitude optical phonons in bismuth, Phys. Rev. B **64**, 092301 (2001).

[13] D. Boschetto, E. G. Gamaly, A. V. Rode, B. Luther-Davies, D. Glijer, T. Garl, O. Albert, A. Rousse, and J. Etchepare, Small atomic displacements recorded in bismuth by the optical reflectivity of femtosecond laser-pulse excitations, Phys. Rev. Lett. **100**, 027404 (2008).

[14] T. Shin, J. W. Wolfson, S. W. Teitelbaum, M. Kandyla, and K. A. Nelson, Carrier confinement and bond softening in photoexcited bismuth films, Phys. Rev. B **92**, 184302 (2015).

[15] S. W. Teitelbaum, T. Shin, J. W. Wolfson, Y.-H. Cheng, I. J. Porter, M. Kandyla, and K. A. Nelson, Real-time observation of a coherent lattice transformation into a high-symmetry phase, Phys. Rev. X **8**, 031081 (2018).

[16] R. Peierls, *More Surprises in Theoretical Physics* (Princeton University Press, Princeton, NJ, 1991).

[17] Y. Liu and R. E. Allen, Electronic structure of the semimetals Bi and Sb, Phys. Rev. B **52**, 1566 (1995).

[18] P. Hofmann, The surfaces of bismuth: Structural and electronic properties, Prog. Surf. Sci. **81**, 191 (2006).

[19] K. Sokolowski-Tinten, C. Blome, J. Blums, A. Cavalleri, C. Dietrich, A. Tarasevitch, I. Uschmann, E. Förster, M. Kammler, M. Horn-von Hoegen, and D. von der Linde, Femtosecond x-ray measurement of coherent lattice vibrations near the Lindemann stability limit, Nature (London) **422**, 287 (2003).

[20] D. M. Fritz, D. A. Reis, B. Adams, R. A. Akre, J. Arthur, C. Blome, P. H. Bucksbaum, A. L. Cavalieri, S. Engemann, S. Fahy, R. W. Falcone, P. H. Fuoss, K. J. Gaffney, M. J. George, J. Hajdu, M. P. Hertlein, P. B. Hillyard, M. Horn-von Hoegen, M. Kammler, J. Kaspar *et al.*, Ultrafast bond softening in bismuth: Mapping a solid's interatomic potential with x-rays, Science **315**, 633 (2007).

[21] G. Sciaini, M. Harb, S. G. Kruglik, T. Payer, C. T. Hebeisen, F.-J. Meyer zu Heringdorf, M. Yamaguchi, M. Horn-von Hoegen, R. Ernstorfer, and R. J. D. Miller, Electronic acceleration of atomic motions and disordering in bismuth, Nature (London) **458**, 56 (2009).

[22] I. Timrov, T. Kampfrath, J. Faure, N. Vast, C. R. Ast, C. Frischkorn, M. Wolf, P. Gava, and L. Perfetti, Thermalization of photoexcited carriers in bismuth investigated by time-resolved terahertz spectroscopy and *ab initio* calculations, Phys. Rev. B **85**, 155139 (2012).

[23] M. Kammler and M. Horn-von Hoegen, Low energy electron diffraction of epitaxial growth of bismuth on Si(111), Surf. Sci. **576**, 56 (2005).

[24] T. Payer, C. Klein, M. Acet, V. Ney, M. Kammler, F.-J. Meyer zu Heringdorf, and M. Horn-von Hoegen, High-quality epitaxial Bi(111) films on Si(111) by isochronal annealing, Thin Solid Films **520**, 6905 (2012).

[25] J. Toudert, R. Serna, I. Camps, J. Wojcik, P. Mascher, E. Rebollar, and T. A. Ezquerra, Unveiling the far infrared-to-ultraviolet optical properties of bismuth for applications in

plasmonics and nanophotonics, J. Phys. Chem. C **121**, 3511 (2017).

[26] See Supplemental Material at http://link.aps.org/supplemental/10.1103/PhysRevB.109.L041105 for additional information on equilibrium ellipsometry measurements.

[27] C. M. Herzinger, B. Johs, W. A. McGahan, J. A. Woollam, and W. Paulson, Ellipsometric determination of optical constants for silicon and thermally grown silicon dioxide via a multi-sample, multi-wavelength, multi-angle investigation, J. Appl. Phys. **83**, 3323 (1998).

[28] H. J. Zeiger, J. Vidal, T. K. Cheng, E. P. Ippen, G. Dresselhaus, and M. S. Dresselhaus, Theory for displacive excitation of coherent phonons, Phys. Rev. B **45**, 768 (1992).

[29] O. V. Misochko, M. Hase, K. Ishioka, and M. Kitajima, Observation of an amplitude collapse and revival of chirped coherent phonons in bismuth, Phys. Rev. Lett. **92**, 197401 (2004).

[30] K. Ishioka, M. Kitajima, and O. V. Misochko, Temperature dependence of coherent A_{1g} and E_g phonons of bismuth, J. Appl. Phys. **100**, 093501 (2006).

[31] T. Shin, Femtosecond reflectivity study of photoacoustic responses in bismuth thin films, Thin Solid Films **666**, 108 (2018).

[32] F. Thiemann, G. Sciaini, A. Kassen, U. Hagemann, F. Meyer zu Heringdorf, and M. Horn-von Hoegen, Ultrafast transport-mediated homogenization of photoexcited electrons governs the softening of the A_{1g} phonon in bismuth, Phys. Rev. B **106**, 014315 (2022).

[33] G. Jnawali, D. Boschetto, L. M. Malard, T. F. Heinz, G. Sciaini, F. Thiemann, T. Payer, L. Kremeyer, F.-J. Meyer zu Heringdorf, and M. Horn-von Hoegen, Hot carrier transport limits the displacive excitation of coherent phonons in bismuth, Appl. Phys. Lett. **119**, 091601 (2021).

[34] A. Hanisch-Blicharski, V. Tinnemann, S. Wall, F. Thiemann, T. Groven, J. Fortmann, M. Tajik, C. Brand, B.-O. Frost, A. von Hoegen, and M. Horn-von Hoegen, Violation of Boltzmann equipartition theorem in angular phonon phase space slows down nanoscale heat transfer in ultrathin heterofilms, Nano Lett. **21**, 7145 (2021).

[35] F. He, E. S. Walker, Y. Zhou, R. D. Montano, S. R. Bank, and Y. Wang, Phase transition in epitaxial bismuth nanofilms, Appl. Phys. Lett. **117**, 073103 (2020).

[36] É. D. Murray, D. M. Fritz, J. K. Wahlstrand, S. Fahy, and D. A. Reis, Effect of lattice anharmonicity on high-amplitude phonon dynamics in photoexcited bismuth, Phys. Rev. B **72**, 060301(R) (2005).

[37] F. Boschini, H. Hedayat, C. Piovera, C. Dallera, A. Gupta, and E. Carpene, A flexible experimental setup for femtosecond time-resolved broad-band ellipsometry and magneto-optics, Rev. Sci. Instrum. **86**, 013909 (2015).

[38] S. Richter, O. Herrfurth, S. Espinoza, M. Rebarz, M. Kloz, J. A. Leveillee, A. Schleife, S. Zollner, M. Grundmann, J. Andreasson, and R. Schmidt-Grund, Ultrafast dynamics of hot charge carriers in an oxide semiconductor probed by femtosecond spectroscopic ellipsometry, New J. Phys. **22**, 083066 (2020).

[39] S. Richter, M. Rebarz, O. Herrfurth, S. Espinoza, R. Schmidt-Grund, and J. Andreasson, Broadband femtosecond spectroscopic ellipsometry, Rev. Sci. Instrum. **92**, 033104 (2021).

[40] C. A. D. Roeser, A. M.-T. Kim, J. P. Callan, L. Huang, E. N. Glezer, Y. Siegal, and E. Mazur, Femtosecond time-resolved dielectric function measurements by dual-angle reflectometry, Rev. Sci. Instrum. **74**, 3413 (2003).

[41] A. M.-T. Kim, C. A. D. Roeser, and E. Mazur, Modulation of the bonding-antibonding splitting in te by coherent phonons, Phys. Rev. B **68**, 012301 (2003).

[42] K. Hricovini, G. L. Lay, A. Kahn, A. Taleb-Ibrahimi, and J. Bonnet, Initial stages of Schottky-barrier formation of Bi/Si(111) and Bi/Si(100) interfaces, Appl. Surf. Sci. **56-58**, 259 (1992).

[43] V. De Renzi, M. G. Betti, and C. Mariani, Quantum size effects and temperature dependence of low-energy electronic excitations in thin Bi crystals, Phys. Rev. B **48**, 4767 (1993).

[44] C. C. Katsidis and D. I. Siapkas, General transfer-matrix method for optical multilayer systems with coherent, partially coherent, and incoherent interference, Appl. Opt. **41**, 3978 (2002).

[45] I. Aguilera, C. Friedrich, and S. Blügel, Electronic phase transitions of bismuth under strain from relativistic self-consistent *GW* calculations, Phys. Rev. B **91**, 125129 (2015).

[46] M. Cardona and D. L. Greenaway, Optical properties and band structure of group IV-VI and group V materials, Phys. Rev. **133**, A1685 (1964).

[47] O. Hunderi, Optical properties of crystalline and amorphous bismuth films, J. Phys. F **5**, 2214 (1975).

[48] S. I. Kudryashov, M. Kandyla, C. A. D. Roeser, and E. Mazur, Intraband and interband optical deformation potentials in femtosecond-laser-excited α-Te, Phys. Rev. B **75**, 085207 (2007).

[49] S. I. Kudryashov, M. Kandyla, C. A. Roeser, and E. Mazur, Transient picometer atomic displacements in α-Te photoexcited by femtosecond laser pulses, in *ICONO 2007: Nonlinear Laser Spectroscopy and High-Precision Measurements; and Fundamentals of Laser Chemistry and Biophotonics*, edited by S. A. Tikhomirov, T. Udem, V. Yudin, M. Pshenichnikov, and O. M. Sarkisov (SPIE, Bellingham, WA, 2007).

[50] H.-L. Liu, T. Yang, J.-H. Chen, H.-W. Chen, H. Guo, R. Saito, M.-Y. Li, and L.-J. Li, Temperature-dependent optical constants of monolayer MoS_2, $MoSe_2$, WS_2, and WSe_2: Spectroscopic ellipsometry and first-principles calculations, Sci. Rep. **10**, (2020).

[51] Z. Han, C. Lee, J. Song, H. Wang, P. Bermel, and X. Ruan, Temperature-dependent full spectrum dielectric function of semiconductors from first principles, Phys. Rev. B **107**, L201202 (2023).

[52] V. Smejkal, C. Trovatello, Q. Li, S. D. Conte, A. Marini, X. Zhu, G. Cerullo, and F. Libisch, Photonic effects in the non-equilibrium optical response of two-dimensional semiconductors, Opt. Express **31**, 107 (2023).

[53] C. Trovatello, F. Katsch, Q. Li, X. Zhu, A. Knorr, G. Cerullo, and S. D. Conte, Disentangling many-body effects in the coherent optical response of 2D semiconductors, Nano Lett. **22**, 5322 (2022).

[54] L. Viña, S. Logothetidis, and M. Cardona, Temperature dependence of the dielectric function of germanium, Phys. Rev. B **30**, 1979 (1984).

[55] P. Lautenschlager, M. Garriga, L. Vina, and M. Cardona, Temperature dependence of the dielectric function and interband critical points in silicon, Phys. Rev. B **36**, 4821 (1987).

[56] P. Lautenschlager, M. Garriga, S. Logothetidis, and M. Cardona, Interband critical points of GaAs and their temperature dependence, Phys. Rev. B **35**, 9174 (1987).

[57] A. I. Shkrebtii, Z. A. Ibrahim, T. Teatro, W. Richter, M. J. Lee, and L. Henderson, Theory of the temperature dependent dielectric function of semiconductors: From bulk to surfaces. Application to GaAs and Si, Phys. Status Solidi B **247**, 1881 (2010).

[58] J. Faure, J. Mauchain, E. Papalazarou, M. Marsi, D. Boschetto, I. Timrov, N. Vast, Y. Ohtsubo, B. Arnaud, and L. Perfetti, Direct observation of electron thermalization and electron-phonon coupling in photoexcited bismuth, Phys. Rev. B **88**, 075120 (2013).

[59] R. Géneaux, I. Timrov, C. J. Kaplan, A. D. Ross, P. M. Kraus, and S. R. Leone, Coherent energy exchange between carriers and phonons in peierls-distorted bismuth unveiled by broadband XUV pulses, Phys. Rev. Res. **3**, 033210 (2021).

[60] M. Hase, K. Mizoguchi, H. Harima, S. I. Nakashima, and K. Sakai, Dynamics of coherent phonons in bismuth generated by ultrashort laser pulses, Phys. Rev. B **58**, 5448 (1998).

[61] T. Shih, M. T. Winkler, T. Voss, and E. Mazur, Dielectric function dynamics during femtosecond laser excitation of bulk Zno, Appl. Phys. A **96**, 363 (2009).

[62] C. König, J. C. Greer, and S. Fahy, Effect of strain and many-body corrections on the band inversions and topology of bismuth, Phys. Rev. B **104**, 035127 (2021).

[63] S. I. Anisimov, B. L. Kapeliovich, and T. L. Perel'Man, Electron emission from metal surfaces exposed to ultrashort laser pulses, Sov. J. Exp. Theor. Phys. **39**, 375 (1974).

[64] A. V. Kuznetsov and C. J. Stanton, Theory of coherent phonon oscillations in semiconductors, Phys. Rev. Lett. **73**, 3243 (1994).

[65] T. E. Stevens, J. Kuhl, and R. Merlin, Coherent phonon generation and the two stimulated raman tensors, Phys. Rev. B **65**, 144304 (2002).

[66] *Light Scattering in Solids 1*, edited by M. Cardona, Topics in Applied Physics Vol. 8 (Springer, Berlin Heidelberg, 1975).